J Mater Sci (2010) 45:4236–4250
DOI 10.1007/s10853-010-4519-z

Nanocrystalline filler induced changes in electrical and stability properties of a polymer nanocomposite electrolyte based on amorphous matrix

Namrata Shukla · Awalendra K. Thakur

Received: 17 February 2010 / Accepted: 12 April 2010 / Published online: 27 April 2010

Abstract An ion conducting polymer nanocomposite electrolyte (PNCE) series of film based on an amorphous polymer host (PMMA)–lithium salt ($LiClO_4$) complex dispersed with nanocrystalline yttria stabilized zirconia (n-YSZ) is reported. X-ray diffraction (XRD) and Fourier transform infrared (FTIR) analysis have confirmed feasibility of interaction among composite components (i.e. polymer–ion–filler). Ions in the PNCE matrix are present in the form of both free cations/anions as well as contact ion pairs and their concentration depends on filler loading in the matrix. Electrical conductivity enhancement on n-YSZ dispersion occurs by $\sim$2 orders of magnitude at 30 °C and by $\sim$5 orders of magnitude at 100 °C when compared with room temperature conductivity of the undispersed polymer salt (PS) film. The highest achieved conductivity value is $\sim 1.3 \times 10^{-4}$ S cm^{-1} at 100 °C for 2 wt% n-YSZ. An excellent correlation between variation of d.c. conductivity and free mobile charge carriers versus filler loading has been observed. This correlation has been attributed to filler-induced polymer–ion–filler interaction. These evidences have formed the basis to propose a mechanism for ion transport.

Introduction

Recently, there has been significant focus on pollution free/green sources of energy. Conversion of chemical energy into electrical energy is one such alternative. The efficient storage of electrical energy needs high energy density batteries having large self-life, high electrochemical potential stability towards electrodes and better conversion efficiency. One of the key components in successful development of high energy density solid state batteries is polymer electrolytes where it serves the dual purpose of a solid electrolyte as well as a separator. However, high ionic conductivity ($\sim 10^{-3}$ S cm^{-1}) at ambient temperature, acceptable mechanical, thermal, interfacial and voltage stabilities are the essential ingredients for device application. A number of approaches have been adopted to develop solid polymeric electrolytes to satisfy the above-mentioned requirements. Literature reports indicate that the homogeneous dispersion of ceramic fillers in the polymer salt (PS) complexes results in an improvement in ionic conductivity and stability properties of polymer electrolyte systems based on poly(ethylene oxide) (PEO)–salt complexes dispersed with inert fillers like Al_2O_3, $BaTiO_3$, TiO_2 and SiO_2 [1–4], etc. Further, the fillers also cause additional improvement in the interfacial stability, rate capability and cyclability [5].

It, therefore, appears that the properties of an ion conducting polymer electrolyte film can be tailored by changing the volume fraction, shape and size of the filler particles [6–8]. There are few reports in literature suggesting desirable improvement in mechanical electrical and thermal properties of solid polymer electrolytes (SPEs) by using nanocrystalline filler with larger aspect ratio [9]. The fillers with dimensions in nanometric level have very large aspect ratio and can be expected to produce desirable enhancement in the conductivity, stability, cyclability and rate capability of the SPEs. In addition, it promotes acceptable improvement in lithium transference number [10, 11], which is one of the important issue for application. This new class of SPE's referred to as polymer nanocomposite electrolytes (PNCEs). The enhancement in

N. Shukla · A. K. Thakur (✉)
Department of Physics and Meteorology, Indian Institute of Technology, Kharagpur 721302, India
e-mail: akt@phy.iitkgp.ernet.in

lithium transference number has been explained by the Lewis acid–base interaction of the ceramic filler surface with the ions (cation/anion) and polymer segment [12–14] in the PNCE matrix. However, the role of nanoceramic fillers as a solid plasticizer or dissociation promoter cannot be ruled out.

Till now, most of the studies on the effect of filler particles have been reported on crystalline-polymer-based SPEs [15]. In this case, a relative decrease in crystallinity on filler addition is believed to be the main reason of conductivity enhancement. On the other hand, the reasons of conductivity enhancement on filler addition in amorphous-polymer-based SPEs is still not well understood.

In the present article, we aim to investigate the role of amorphous polymer host on changes in the conduction and stability properties of ion conducting film based on poly (methyl-methacrylate) (PMMA). The effect of nanocrystalline yttria stabilized zirconia (n-YSZ) dispersion on tailoring of d.c. conductivity and stability properties of the PNCE series of film is analyzed. A systematic study of filler-induced ion–ion and ion–polymer interaction has provided significant basis to propose a model for ion transport behaviour in the PNCE films. The concept of the model appears to be consistent with the experimental results.

Experimental

PNCE films were prepared by means of a standard solution cast technique over a range (0–20 wt%) of nanofiller (n-YSZ) dispersed in PMMA–$LiClO_4$ matrix.

PMMA (Aldrich M.W. $\simeq 2 \times 10^5$) was used as the polymer host matrix, $LiClO_4$ (Acros organics USA) as the salt for complexation and yttria stabilized zirconia (Aldrich), having average particle size $\simeq$50 nm and appreciably high specific surface area $\simeq$60 m^2/g, as the filler for dispersion. The polymer host (PMMA) was vacuum-dried and the salt ($LiClO_4$) was dried at a temperature $\simeq$150 °C for 24 h to remove surface absorbed moisture content prior to sample preparation. An appropriate stoichiometric ratio of PMMA was dissolved in acetonitrile (Merck) and the solution was stirred for 12 h. Subsequently, calculated amount of $LiClO_4$ was added and stirred for 12 h to facilitate homogeneous mixing and complexation. Finally, the stoichiometric ratio of n-YSZ (x), expressed as

$$x\% = \left(\frac{\text{wt. of n} - \text{YSZ}}{\text{wt. of PMMA}}\right) \times 100,$$

has been added to the PS solution and again stirred for 12 h. The resulting composite solution, comprising of polymer–salt–filler components, for each filler concentration was cast into films in polypropylene dishes and the solvent was allowed to evaporate slowly at room temperature (27 °C). The solvent evaporated free standing polymer nanocomposite (PNCE) films were finally vacuum-dried at 40 °C to remove residual solvent, if any, and stored in an inert medium for further analysis.

The X-ray diffraction (XRD) pattern were recorded at room temperature using Philips X'Pert Pro PANalytical diffractometer (Model: PW 3040/60) with Cu Kα radiation ($\lambda = 1.5418$ Å) over a range of diffraction angles; $10° \leq 2\theta \leq 60°$ at a scanning rate $\sim 4°$ min^{-1}. Fourier Transform Infrared (FTIR) Spectrum were collected in the mid-frequency range (4000 to 400 cm^{-1}) at an average scan rate of 32 using Thermo Nicolet Spectrophotometer (Model: NEXUS–870). Complex impedance spectrum (CIS) measurements on the PNCE series of films were performed using a computer interfaced impedance analyzer (HIOKI LCR Hi-Tester, Model: 3532, Japan) in the frequency range of 100 Hz to 1 MHz. The sample cells having a configuration; SS|PNCE|SS were placed in a self-designed sample holder for electrical measurements (SS stands for stainless steel blocking electrodes). An a.c. input signal of $\sim$200 mV (peak to peak) was applied across the cell prior to start of the electrical measurements. Sample microstructure has been studied by high resolution transmission electron microscopy (HR-TEM) analysis using JEOL-JEM (model: 2100, Japan).

Results

XRD analysis

Figure 1 shows the XRD pattern of n-YSZ dispersed PNCE films. The XRD pattern of PS complex has low intensity diffused (weak) peaks at diffraction angles (2θ) $\sim$ 16.2°, 30.6° and 41.2°. All the peaks are diffused suggesting highly amorphous nature of the samples [16]. On filler dispersion, additional peaks appear at $2\theta \sim$ 30°, 34.8°, 50.2° and 60°. They are indexed as (111), (200), (220), and (311), respectively, and indicate the presence of filler as a separate phase in the composite matrix. In addition, polymer peaks undergo drastic modification in their intensity at higher filler concentration. The effect of filler concentration on PS complex has been observed by analyzing the changes in the main profile of PMMA peak ($2\theta = 16.2°$) and main ZrO_2 peak ($2\theta \sim 30°$). The d-spacing and interchain separation of the PMMA peak has been calculated using the following relations considered to be valid for non-crystalline solids:

$$d\text{-spacing} \quad d = \frac{\lambda}{2\text{Sin}\theta}$$

$$\text{Interchain separation} \quad R = \frac{5\lambda}{8\text{Sin}\theta},$$

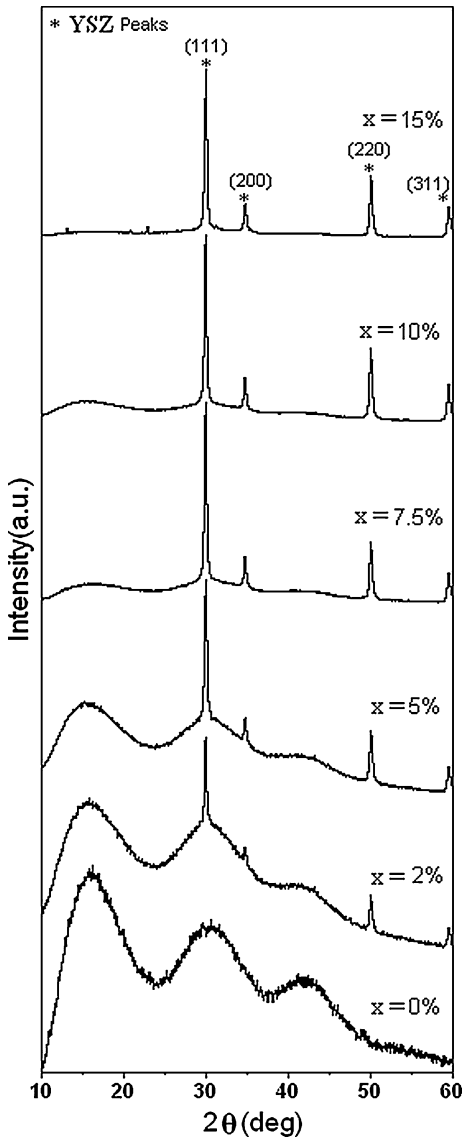

Fig. 1 XRD pattern of $PMMA_4$–$LiClO_4$ + x wt% nano-YSZ-based PNCE films

where λ and θ are wavelength of X-rays (1.5418 Å) and angle, respectively. The effect of n-YSZ dispersion on the position, width and intensity of PMMA main peak are shown in the Table 1. The peak position is almost the same over a range of filler concentration varying from 0 to 7.5 wt% (w/w of PMMA). However, for n-YSZ >7.5 wt% the peak appears to shift towards lower angle (2θ) side of the XRD pattern. The d-spacing as well as the interchain separation of the polymer host remains almost unaffected when the filler concentration is increased up to 10 wt%. However, for $x \geq 10$ wt% a mild increase in d-spacing as well as the interchain spacing has been observed. It can be considered to be well within the limit of experimental errors.

The changes in the diffraction profile of the (d_{111} peak) of n-YSZ on dispersion in the PS matrix is shown in Fig. 2 and compared with that of the n-YSZ powder. A comparison indicates that the n-YSZ d_{111} peak position undergoes a small shift towards low angle side on addition of small amount of filler ($\sim$1 wt%). Beyond this concentration limit, the n-YSZ peak position remains unaffected with further increase in the filler concentration (>1 wt%). Although the d-spacing of n-YSZ remains almost invariant with filler loading, the full width half maxima (FWHM) shows significant variation with the concentration of n-YSZ filler (Table 2).The above result provides convincing evidence for mutual interaction between the PS complex matrix and nano-YSZ filler.

Fourier transform infrared spectroscopy analysis

FTIR spectroscopy is a powerful tool to probe the possibility of nanoceramic filler-induced interaction among composite components, i.e. ion–ion and ion–polymer interaction. The internal mode of the salt, $LiClO_4$, is particularly sensitive to the local anionic (ClO_4^-) environment [17, 18]. In free (uncoordinated) state, the ClO_4^- ion exhibits 9 ($3N - 6$;

Table 1 Changes in the preliminary structural parameters of the host polymer (PMMA) with increase in n-YSZ loading

n-YSZ Concentration variation (x wt%)	Peak position	XRD main peak of PMMA		
		d-Spacing $d = \lambda/2\sin\theta$ (Å)	Relative intensity (I_{Comp}/I_{PS})	R (interchain separation) $R = 5/8(\lambda/\sin\theta)$ (Å)
0	16.2	5.5	100	6.8
1	16.2	5.5	95	6.8
2	16.2	5.5	94	6.8
5	16.1	5.5	92	6.8
7.5	16.2	5.5	88	6.8
10	16.0	5.5	90	6.8
15	15.8	5.6	90	7.0
20	15.8	5.6	90	7.0

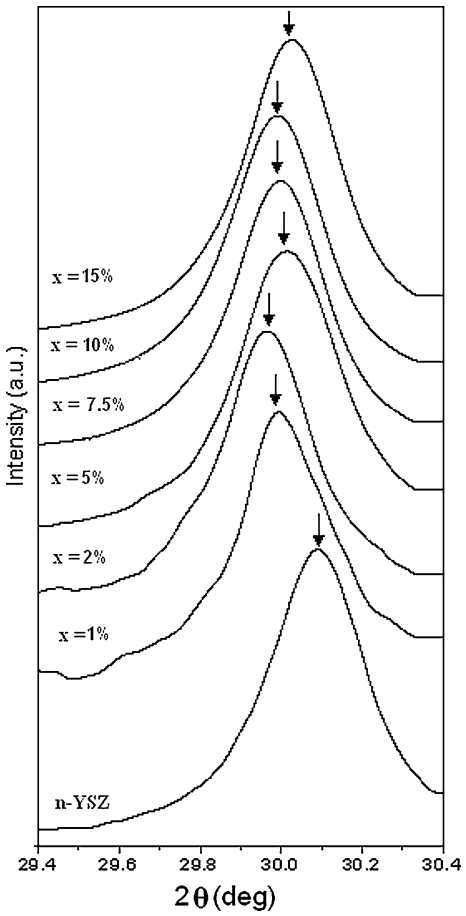

Fig. 2 Shifting of YSZ (111) XRD peak in $PMMA_4$–$LiClO_4$ + *x* wt% nano-YSZ-based PNCE films

Table 2 Changes in the diffraction peak profile of (111) peak in the PNCE films on comparison with n-YSZ powder

Filler concentration (*x* wt%)	Peak position ($2\theta°$)	FWHM × 10^3 (rad)	*d*-Spacing (Å)
Nanopowder-YSZ	30.1	4.2	2.9
1	30.0	4.4	3.0
2	30.0	4.4	3.0
5	30.0	5.1	3.0
7.5	30.0	4.7	3.0
10	30.0	4.7	3.0
15	30.0	4.7	3.0
20	30.0	4.5	3.0

$N = 5$) fundamental vibrational modes arising out of its tetrahedral symmetry (T_d). All the modes including the degenerate (i.e. $T_2 \sim 625\ cm^{-1}$, $T_2 \sim 1{,}100\ cm^{-1}$ and $E_1 \sim 460\ cm^{-1}$) and the nondegenerate (i.e. $A_1 \sim 910\ cm^{-1}$) are Raman active. On the other hand, the modes observed at T_2 ($\sim$625 cm^{-1}), T_2 ($\sim$1100 cm^{-1}) are IR active. They are attributed to uncoordinated ClO_4^- anion

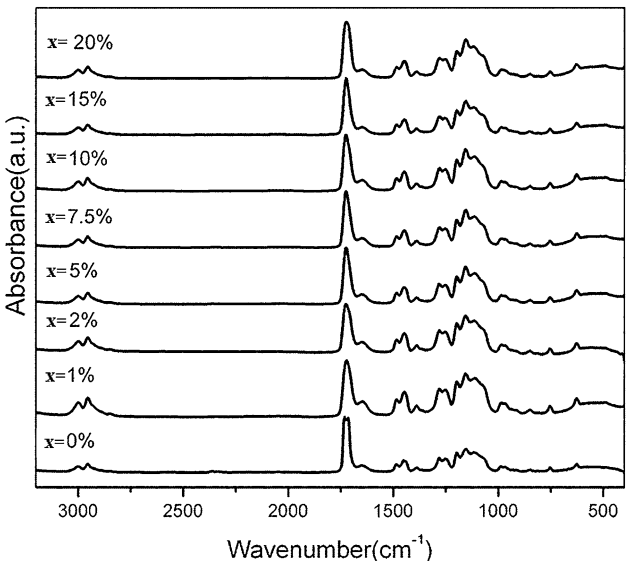

Fig. 3 Fourier transform infrared (FTIR) pattern of $PMMA_4$–$LiClO_4$ + *x* wt% nano-YSZ-based PNCE films

[19, 20]. The free ClO_4^- anion symmetry undergoes drastic changes from $T_d \rightarrow C_{3v}$ or $T_d \rightarrow C_{2v}$ on interaction with the counter ions. The simple ion pairs ($Li^+ClO_4^-$) and higher ion aggregates/multiples [$Li_2ClO_4^-/Li^+(ClO_4)_2$] give rise to symmetry lowering from $T_d \rightarrow C_{3v}$ and $T_d \rightarrow C_{2v}$, respectively.

Figure 3 shows the FTIR spectra of PNCE films with different filler concentration. A detailed assignment of the experimentally observed FTIR bands attributed to the vibrational modes of various molecular groups in the composite film is shown in Table 3. The characteristic bands of PMMA appearing at 760, 1140, 1270, 1732 and 2845 cm^{-1} are due to $\gamma(CH_2)$ [21], $\delta(CH_2)$, $\nu_a(C–O)$, $\nu(C=O)$ and $\nu(CH_2)$ [22], respectively. On addition of salt in the host polymer (PMMA), additional peaks appear at 487, 625 cm^{-1} and a weak shoulder at 1665 cm^{-1}. The peaks at 487, 625 cm^{-1} are attributed to $\delta_s(ClO_4^-)$ and $\delta_a(ClO_4^-)$, respectively [23]. Further the spectral pattern shows noticeable changes in the vibrational modes of PMMA and $LiClO_4$ in terms of shift in their band positions, band width and intensity on addition of filler (Table 3). These changes in the vibrational modes provide preliminary evidence of PMMA, $LiClO_4$ are clear evidence of polymer–salt–filler interaction. A detailed analysis of such polymer–ion–filler interaction is discussed in the following section.

Polymer–ion interaction

It appears from the FTIR spectrum (Fig. 3) that the vibrational bands of PMMA at 760, 1192, 1271, 1492 and 1732 cm^{-1} appear to be affected on salt addition to the

Table 3 Fourier transform infrared band identification and assignment for PNCE films based on $PMMA_4$–$LiClO_4$ + x wt% nano-YSZ

PMMA	$x = 0$	$x = 1$	$x = 2$	$x = 5$	$x = 7.5$	$x = 10$	$x = 15$	$x = 20$	Assignment
	487	488	488	489	489	489	489	491	$\delta_s(ClO_4^-)$
–	626	626	626	626	626	626	626	626	$\delta_a(ClO_4^-)$
760	751	753	753	753	753	753	753	753	$\gamma(CH_2)$
844	846	849	849	849	848	849	849	849	$\gamma_a(CH_2) + \nu_s$(C–O–C)
989	986	985	985	984	984	984	984	983	$\gamma(CH_2$–CH) + ν_S(C–C)
	1112	1112	1115	1112	1113	1113	1116	1117	$\nu_a(ClO_4^-)$
1150	1153	1155	1155	1155	1155	1155	1155	1154	$\delta(CH_2)$
1192	1197	1197	1197	1197	1197	1197	1197	1196	ν_S(C–H), C–O–C bending
1242	1242	1251	1252	1251	1251	1251	1252	1252	$\nu_S(OCH_3)$ C–C–O stretch
1271	1280	1280	1280	1280	1280	1280	1280	1279	ν_a(C–O) in –COO– group
1387	1387	1388	1388	1388	1388	1388	1388	1388	$\tau(CH_2)$ C–CH_3 bending
1444	1444	1446	1446	1446	1447	1447	1447	1448	C–O–C and ν_a(O–CH_3)
1492	1485	1483	1483	1483	1483	1483	1483	1482	$\delta_a(CH_2)$
1732	1728	1722	1723	1723	1723	1723	1723	1723	ν(C=O)
2845	2845	2847	2847	2847	2848	2847	2847	2848	$\nu(CH_2)$
2951	2954	2954	2954	2954	2954	2954	2954	2954	ν_s(C–H) of C–CH_3
2999	2999	2998	2998	2999	2999	2999	2999	2999	ν_a(C–H) of O–CH_3

PMMA matrix. The changes in the band position suggest possibility of polymer interaction with cations of the salt due to PS complex formation. On complexation with salt, the polymer (PMMA) peaks at 760, 1492 and 1732 cm^{-1} have shifted towards lower wavenumber side (751, 1485 and 1728 cm^{-1}) while the peaks at 1192 and 1271 cm^{-1} have shown opposite trend with a shift towards the higher wavenumber side (1197 and 1280 cm^{-1}). Appearance of new shoulder at 1665 cm^{-1} in addition to the noticeable asymmetry in the ν(C=O) (Fig. 4a) band suggests clear evidence of polymer–ion interaction in the PS film due to cation (Li^+) coordination at C=Ö site of the polymer chain [24]. Hence, the changes in the FTIR band of the host polymer PMMA evidently support the possibility of Coulombic interaction between the cation and highly reactive group (–COO–) of PMMA suggesting strong polymer–ion interaction. This result on polymer–ion interaction appears to be consistent with previous reports in literature [25].

Polymer–filler interaction

Figure 4a, b shows changes in the position of ν(C=O) band and changes in the profile of $\nu_s(OCH_3)$, vibrational mode of the polymer chain, respectively. The changes in ν(C=O) band position as a function of filler has been shown in Fig. 4a. The band attributed to ν(C=O) is present at 1728 cm^{-1} in the PS film. On addition of 1 wt% of the filler a shift in the band position occurs from 1728 to 1722 cm^{-1}. With increase the n-YSZ loading higher than 1 wt%, the new position appears at 1723 cm^{-1} and it remains unaffected for the remaining PNCE (2–20 wt% filler) films. In addition to shifting, a broadening of ν(C=O) peak of the PS film is also observed. The shifting of ν(C=O) towards lower wavenumber side on addition of filler demonstrates that the polymer carbonyl (>C=O) groups are affected due to direct interaction with the nano-YSZ filler. A similar result has also been reported previously [26]. It seems that addition of filler has drastically changed intensity profile of the shoulder 1665 cm^{-1}. Dispersion of even 1 wt% filler causes the shoulder to shift towards lower wavenumber side ($\sim$1644 cm^{-1}) (Fig. 4a). This change occurs in a systematic fashion on subsequent change in filler concentration and suggests clear evidence of ion–filler interaction.

Figure 4b shows the FTIR spectral bands, attributed to ν_s(O–CH_3) mode of the host polymer PMMA. On addition of filler, the band position of ν_s(O–CH_3) mode undergo shift towards higher wavenumber side and also exhibit broadening. The changes in the FTIR spectral bands, attributed to ν_s(O–CH_3) and ν(C=O) modes of the host polymer, with nanofiller concentration provide convincing evidence for strong polymer–filler interaction in the PNCE film.

Ion–ion interaction

Figure 5 shows the spectral pattern of perchlorate (ClO_4^-) group in the wavenumber region of 600–650 cm^{-1}. The peak profile is observed to change considerably indicated

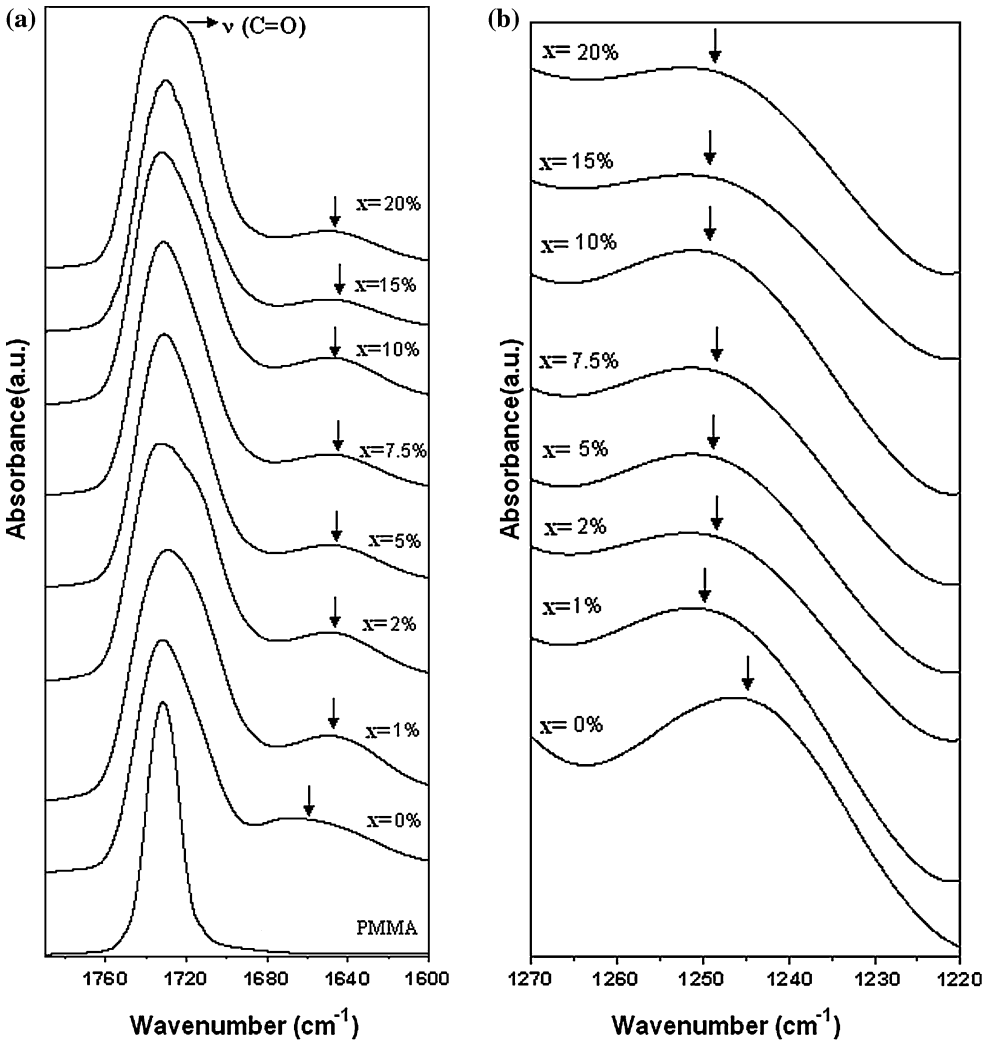

Fig. 4 **a** Changes in the profile of υ(C=O) band of PMMA on dispersion of x wt% nano-YSZ filler. **b** Changes in vibrational peak profile of $\nu_s(OCH_3)$ band of PS matrix on dispersion of x wt% nano-YSZ filler

by changes in the intensity and peak profile with filler loading. The asymmetry in the band profile arises due to resolved degeneracy of the $\delta_a(ClO_4^-)$ mode in both the PS and PNCE films. This resolved degeneracy in the pattern of $\delta_a(ClO_4^-)$ reveals the coordination of ClO_4^- group with counterion to form the ion pair (solvent separated/contact ion pairs, i.e. M^+X^-) and higher ion aggregate ($M_2^+X^-$). In general, any possible interaction of free ClO_4^- group with counter ions that causes formation of ion pair or higher ion aggregate, results in band asymmetry or appearance of additional peaks in the spectral band region for T_2 vibrational modes (624/1100 cm^{-1}) [27]. Deconvolution of the ClO_4^- bands occurring at 624 cm^{-1} may give three degenerate bands appearing at 624, 635 and 637 cm^{-1}. They are attributed to the free ion, contact ion pair and ion aggregates, respectively. In the present studies, the last possibility could not be witnessed. The presence of E_1 vibrational mode of ClO_4^- anion observed at $\sim$481 cm^{-1} is the clear evidence of change of symmetry of ClO_4^- from $T_d \rightarrow C_{3v}$, i.e. the presence of uncoordinated ClO_4^- free anion and ion pairs [28].

Polymer–ion–filler interaction

The variation in the intensity, peak shape and position of band profile of $\delta_S(ClO_4^-)$, $\delta_a(ClO_4^-)$ (Fig. 6) and $\nu_a(ClO_4^-)$ with the variation in filler loading, provide clear evidence for feasibility of interaction among polymer–ion and filler components of the composite. The polymer–ion–filler interaction in the nanocomposite films has been revealed by asymmetry in the (ClO_4^-) band in the spectrum at wavenumber $\sim$624 cm^{-1}. The observed asymmetry in the FTIR band of 624 cm^{-1} requires deconvolution to ascertain its origin. Deconvoluted pattern, shown in Fig. 6, indicates two contributions at 624 and 635 cm^{-1}. The bands at 624 and 635 cm^{-1} are attributed to the free ion and contact ion pairs, respectively. The deconvoluted ClO_4^- band can be used to quantify the fraction of free anion

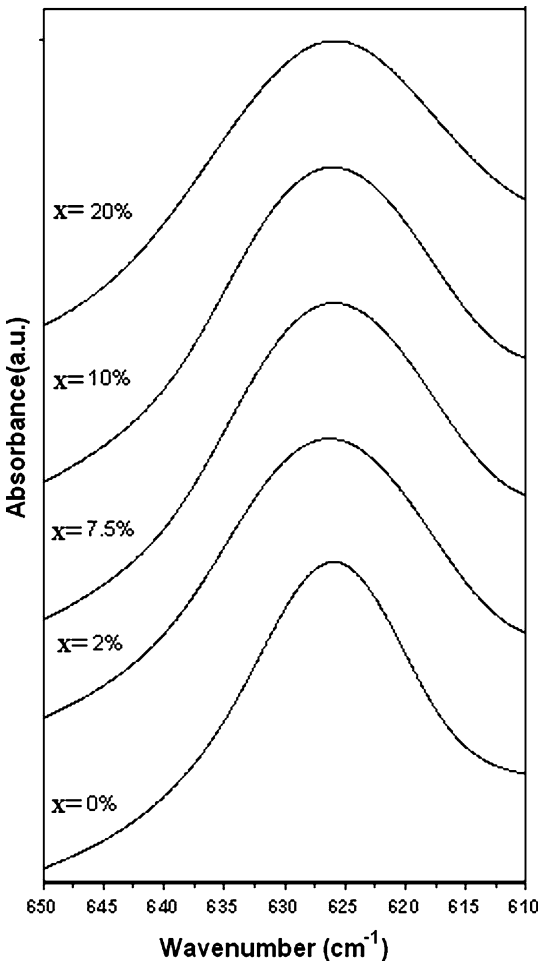

Fig. 5 Effect of n-YSZ concentration on changes in the absorption band profile of $\delta(ClO_4^-)$ vibrational mode in PNCE films of composition $PMMA_4$–$LiClO_4$ + x wt% nano-YSZ-based PNCE films

(FFA) and ion pair (FIP) in accordance with the following formula:

$$\text{FFA} = \frac{\text{Free anion peak area}}{\text{Total peak area}} \quad \text{FIP} = \frac{\text{Ion pair peak area}}{\text{Total peak area}}$$

The FFAs gives a direct measure of the free mobile charge carriers (i.e. Li^+) available for conduction, therefore, provides significance information relating the ion transport properties. A variation pattern of the FFA and ionic conductivity as a function of filler (n-YSZ) concentration, indicate that the FFA increases for PNCE films with low filler concentration (1–2 wt%). The PNCE film with 2 wt% filler loading has a highest value of free cations. The typical variation of free anion fraction as a function of filler (n-YSZ) is later compared with that of the d.c. conductivity.

Complex impedance spectroscopy analysis

Figure 7 shows CIS for the PS and PNCE films at room temperature (30 °C). The CIS pattern of PS film comprises of a depressed semicircular arc attributed to the bulk contribution. The depressed semicircular arc is electrically equivalent to a parallel arrangement of resistance (R), capacitance (C) and constant phase element (CPE). The impedance of CPE can be expressed mathematically as

$$Z_{\text{CPE}} = \frac{1}{Q_0(J\omega)^n},$$

where Q_0 and n are the fitting parameters. Their values determine the sample electrical response as an electrical analogue of resistance, Warburg impedance, capacitance and inductance for different values of $n = 0, 0.5, 1$ and -1, respectively. The angle θ by which the semicircular arc is depressed below the real axis is related to the width of the relaxation time distribution (α) and its value is given by $\alpha = (1 - n)\pi/2$. The true value of capacitance can be calculated by the expression given by Hsu and Mansfeld $C = Q_0(\omega_{\max})^{n-1}$ [29]. The CPE in a heterogeneous sample arises because of microstructural inhomogeneity, presence of multiphase regions, local charge inhomogeneity and variation in phase composition/stoichiometry. The inhomogeneity in the material indicates the nonuniform charge mobility through the sample due to different mobility rates in various micro regions comprising of different local phases in the sample. This seems logical in view of different values of impedance associated with CPE and their exponents 'n'.

On nanoscopic dispersion of n-YSZ filler particle in PS matrix, a clear change in the evolution pattern of CIS spectrum is noticed. The PNCE films with nanodispersed filler (2–7.5 wt% filler dispersion) shows a depressed semicircular arc at high frequency followed by a small spike at low frequency. The first depressed semicircular arc is due to the bulk contribution whereas the small spike is due to the presence of space charge polarization. Its electrical analogue represents a more complex circuit comprising of one parallel arrangement of resistance (R), capacitance (C) and CPE in series with another CPE. The calculated value of capacitance from this spike is $\sim$0.01 μF. It confirms the contribution of space charge polarization at the material electrode interface. The CPE values of bulk sample have relatively lower magnitude of interfacial polarization. The presence of CPE in the impedance response suggests marked departure from the Debye like behaviour. The Q and n values indicate that the CPE attributed to the bulk semicircle behaves more like a capacitor. The fitted value of capacitance on electrical equivalent circuit in the experimental impedance plot is of the order of $\sim$pF. This suggests that capacitive component in the circuit is a response from the bulk interior. The fitted data appears to be consistent with the interpretation of the single semicircular arc in the CIS pattern. On addition of the filler, the resistance of the bulk sample decreases up to 7.5 wt% filler loading. Further increase in the filler concentration

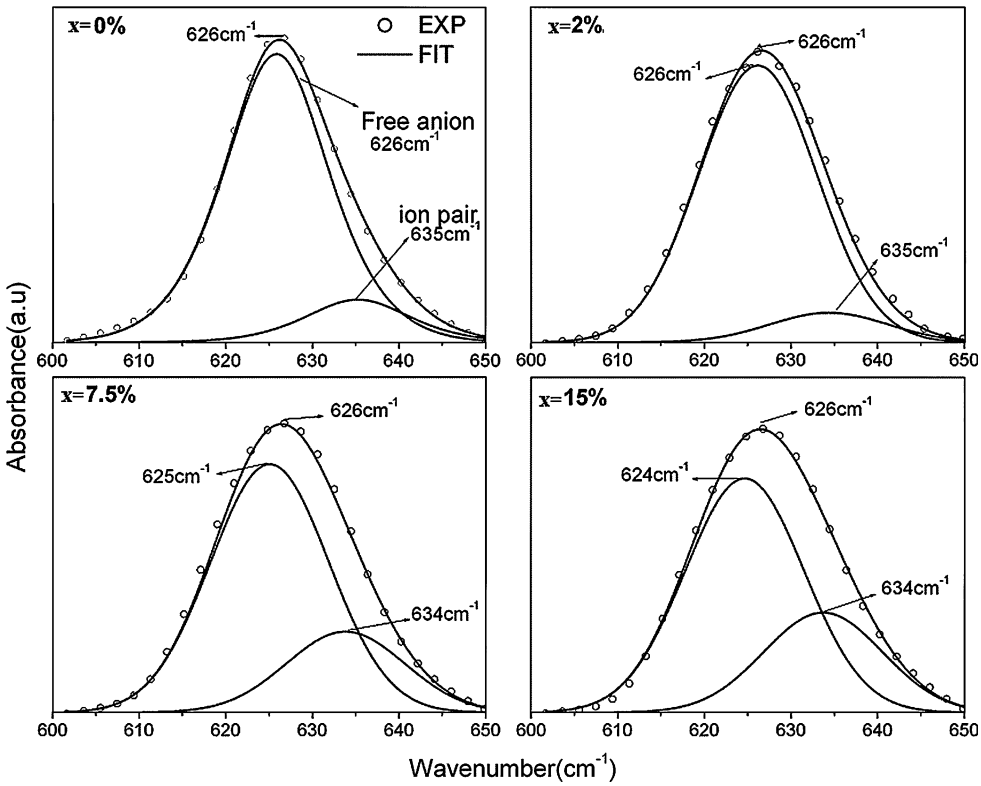

Fig. 6 Deconvoluted profile of perchlorate band displaying of the individual contribution due to free anion and ion pair in $PMMA_4$–$LiClO_4$ + x wt% nano-YSZ-based PNCE films

(>7.5 wt%) increases the bulk resistance. As the amount of filler increases from 7.5 wt%, the CIS pattern again shows one single depressed semicircular arc and their electrical equivalent agrees well with that of the PS film (i.e. it also comprises of the parallel arrangement of resistance (R), capacitance (C) and CPE. The faster ion dynamics causing accumulation of charges at the interface of the PNCE samples with 2, 5 and 7.5 wt% n-YSZ loading. For PS and PNCE films with higher filler loading (≥7.5 wt%) charge transport is relatively slower. Hence, accumulation of charge at the interface is relatively not so effective.

As the temperature rises, the CIS pattern undergoes substantial changes and for all the samples (PS and PNCE), the CIS spectrum profile comprises of a semicircular arc in the high frequency region followed by a steep spike in low frequency region. The CIS of PS and PNCE films at high temperature (100 °C) is shown in the Fig. 8. A comparison of the CIS spectrum and their corresponding electrical equivalent circuit with that in Fig. 7 indicates that (i) for all the samples (PS and PNCEs) the electrical equivalent circuit consists of one parallel arrangement of resistance (R) and CPE is in series with another CPE. (ii) The resistance value for all the samples is almost three orders of magnitude less than at room temperature. (iii) The double layer capacitance (C_{dl}) value is higher at 100 °C. The latter is a natural consequence of relatively higher mobility of the charge carriers at elevated temperatures. It causes accumulation of charge carriers at the electrode electrolyte interface resulting in a decrease in resistance and consequent increase in C_{dl}. At 100 °C, the estimated value of C_{dl} is found 0.1 μF for PS film and 1–2 μF for the PNCE films with 2–7.5 wt% filler loading. The magnitude of the double layer capacitance (C_{dl}) has been calculated from the equation:

$$C_{dl} = \frac{1}{2\pi f Z''},$$

where f is the frequency and Z'' is imaginary part of the impedance. For all the samples, the CPE values of bulk samples are invariably lesser than the CPE values due to interfacial polarization. The value of n is near to 1 which indicates that CPE due to bulk behaves like a capacitor.

Electrical conductivity

The electrical conductivity has been calculated using the value of bulk resistance (R_b), estimated from the intercept of the high frequency arc on the real axis of the CIS. The variation of σ_{dc} as a function of filler concentration at 30 and 100 °C is shown in Fig. 9. The common features at 30 and 100 °C are: (i) the conductivity increases on addition of even small amount of filler (1–2 wt%) showing a maxima, (ii) electrical conductivity gets lowered on subsequent filler addition (5 wt%), (iii) another maxima in the conductivity variation pattern occurs at intermediate filler concentration (7.5 wt%) and (iv) a

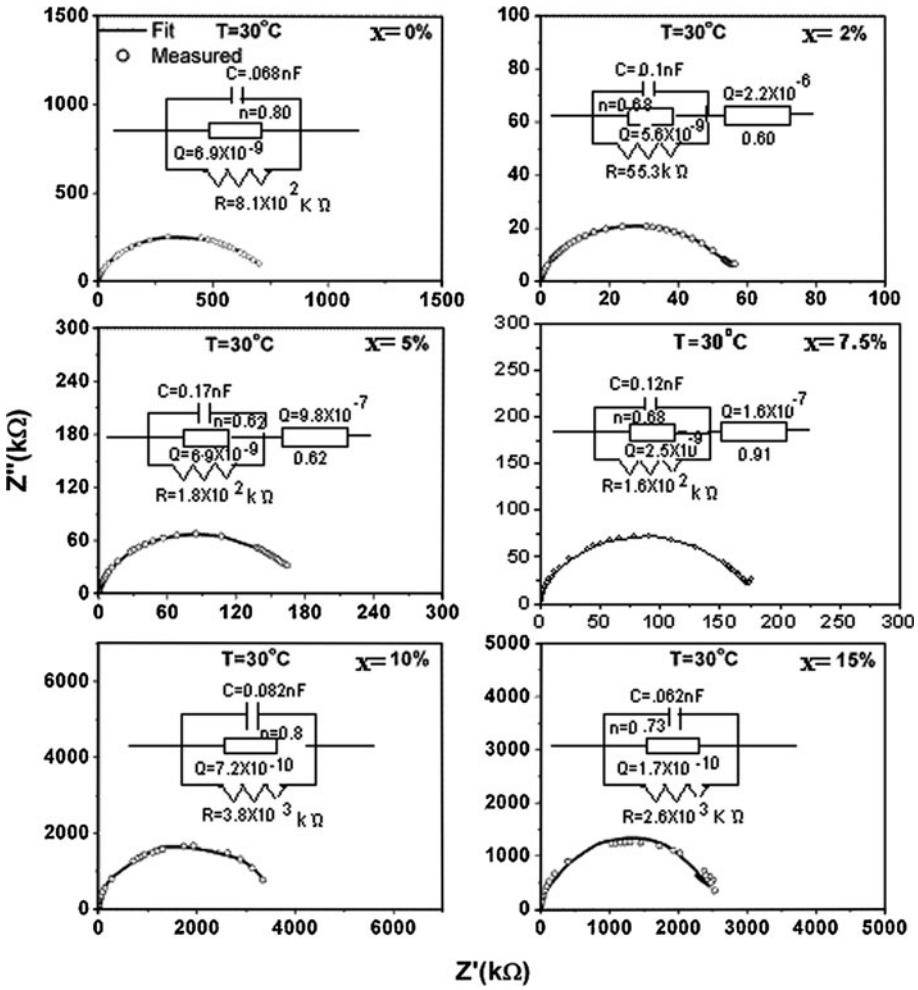

Fig. 7 Room temperature ($T = 30$ °C) complex impedance plot for PNCE films of composition $PMMA_4$–$LiClO_4 + x$ wt% nano-YSZ

monotonous decrease in conductivity takes place for the filler loading ≥7.5 wt%. At 30 °C, an enhancement in conductivity occurs by two orders of magnitude at 2 and 7.5 wt% filler concentration when compared with that of the undispersed PS film. At 30 °C, the PNCE films with the filler loading 1–7.5 wt% show significantly higher conductivity than the PS film. As the filler loading increases (>7.5 wt%), the conductivity value decreases and it becomes lower than the PS film. The highest value of conductivity $\sim 2.6 \times 10^{-7}$ S cm^{-1} has been observed for low filler loading (2 wt%). At 100 °C, which equals polymer glass transition temperature, the two maxima features of conductivity occurring at 2 and 7.5 wt% of filler dispersion are retained. However, a substantial enhancement in conductivity by ~ 1 order of magnitude is observed in the composite films when compared with undispersed PS film. The highest achieved conductivity value is $\sim 1.3 \times 10^{-4}$ S cm^{-1}. This drastic jump in conductivity at 100 °C may be related to the combined effect of flexibility of polymer chains as well as larger fraction of free mobile charge carriers (free anion and hence free cation) at specific filler concentration.

This change in conductivity agrees well with the FFA versus filler concentration pattern (Fig. 9). On the basis of this excellent correlation between the conductivity and available free mobile charge carrier in the PNCE matrix at specific filler loading, a mechanism of ion conduction has been proposed. It is discussed later in this manuscript.

Ion transport properties

The ionic transport number 't_{ion}' has been estimated using Wagner's d.c. polarization technique at a fixed applied voltage (80 mV) across the sample cell. The variation in the polarization current as a function of time is shown in Fig. 10. The pattern of variation shows a high initial current (I_t) followed by the attainment of saturation current (I_e) after a few hours. The ionic and electronic contribution to the conductivity has been estimated by the following relation. It is shown in Table 4.

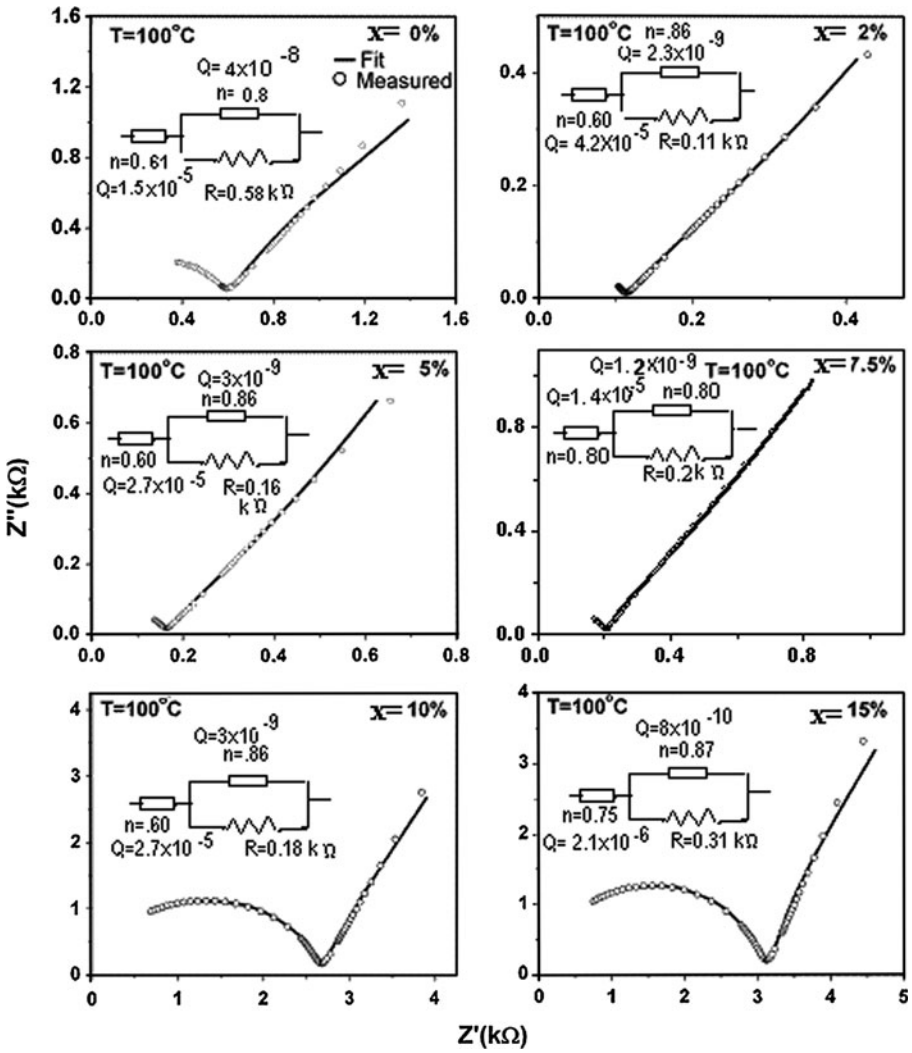

Fig. 8 Complex impedance plot at high temperature ($T = 100$ °C) for PNCE films of composition $PMMA_4$–$LiClO_4 + x$ wt% nano-YSZ

$$t_{\text{ion}} = \left(\frac{I_t - I_e}{I_t}\right) \times 100$$

$$t_{\text{ion}} + t_e = 1$$

The ionic transport number (t_{ion}) value obtained has been found ~99% which indicates that PS and PNCE films are predominantly ionic conductor.

Voltage stability

A variation of the residual electronic current as a function of applied d.c. bias for the PS and PNCE films are shown in the Fig. 11. For PS film the residual current increases gradually till the applied voltage is around ~3.1 V. Beyond this voltage limit, the current rises suddenly with an increase of three orders of magnitude. The voltage at which the residual electronic current shoots up to a very high value is called the breakdown voltage and upper limit of this voltage gives a measure of the 'working voltage limit'. The same behaviour is found in the case of nanocomposite films with relatively higher value of breakdown voltage. PS film shows voltage stability limit ~3.1 V. On addition of small amount of filler (1–2 wt%) into the PS matrix causes an increase in the voltage stability value (4 V) and it goes on increasing with increase in the filler concentration. The PNCEs with 7.5–10 wt% filler have the highest value of voltage stability 4.5 V. However, the reason for enhancement in voltage stability is not known till date.

Discussion

The correlation between the variation in d.c. conductivity and the changes in the FFA and FIP as a function of nanoceramic filler (nano-YSZ) concentration provides enough of evidence to propose a mechanism for filler-induced conductivity enhancement and ion transport. The essence of mechanism lies in a direct interaction of nano-

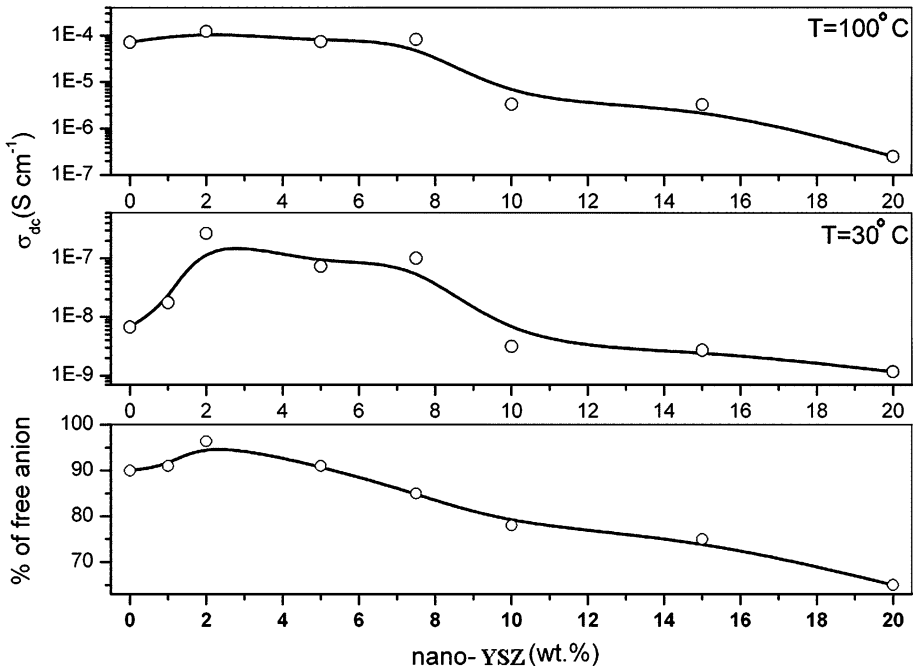

Fig. 9 A comparative plot showing variation of free anion fraction (%) and d.c. conductivity at room temperature and 100 °C

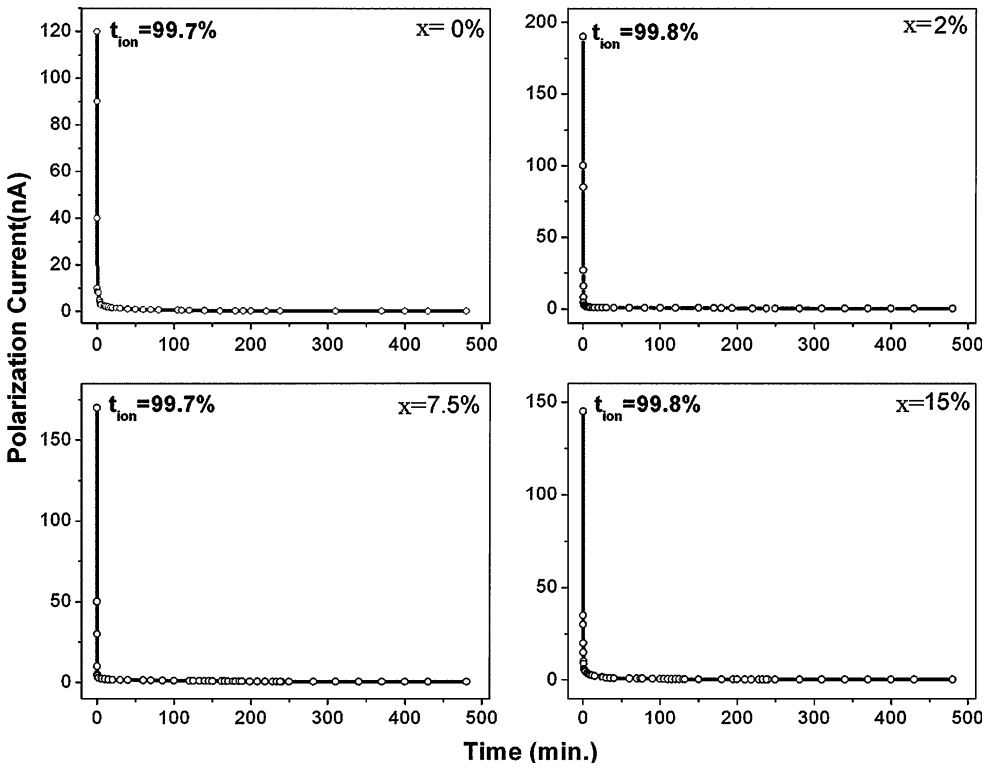

Fig. 10 Variation of polarization current as a function of time under a constant applied voltage ($V = 80$ mV) for PNCE films of composition $PMMA_4$–$LiClO_4 + x$ wt% nano-YSZ

YSZ with both the polymer host and the conducting species (i.e. Li^+/ClO_4^-) in the composite matrix. This interaction, evidenced from FTIR analysis, seems reasonable as well as feasible in view of very high permittivity of nano-YSZ (~25–30) [30] in comparison to $\varepsilon_r \sim 3$–4 for the host polymer holding cations at its electron rich carbonyl oxygen sites (C=Ö). In addition, the hard Lewis acid character of n-YSZ acts as a catalyst for filler interaction with the polymer host at its electron rich site as well as the anion ClO_4^- in the matrix. The latter as a Lewis base. The overall effect of interaction is release of charge carriers with freedom of mobility. The various steps, via which this process may be occurring, are presented schematically in the Fig. 12a–e.

Table 4 Ionic transport number, electronic transport number, calculated values of ionic and electronic conductivity and voltage stability for PNCE films

n-YSZ (wt%)	Ionic transport number (%)	Electronic transport number (%)	Ionic conductivity (S cm^{-1})	Electronic conductivity (S cm^{-1})	Voltage stability
0	99.7	0.30	6.68×10^{-9}	2.0×10^{-11}	3.1
2	99.8	0.20	2.69×10^{-7}	5.4×10^{-11}	4.0
5	99.7	0.30	7.27×10^{-8}	2.2×10^{-10}	4.2
7.5	99.7	0.30	9.98×10^{-8}	2.0×10^{-10}	4.5
10	99.7	0.30	3.09×10^{-9}	9.3×10^{-12}	4.5
15	99.8	0.20	2.69×10^{-9}	5.4×10^{-12}	4.4

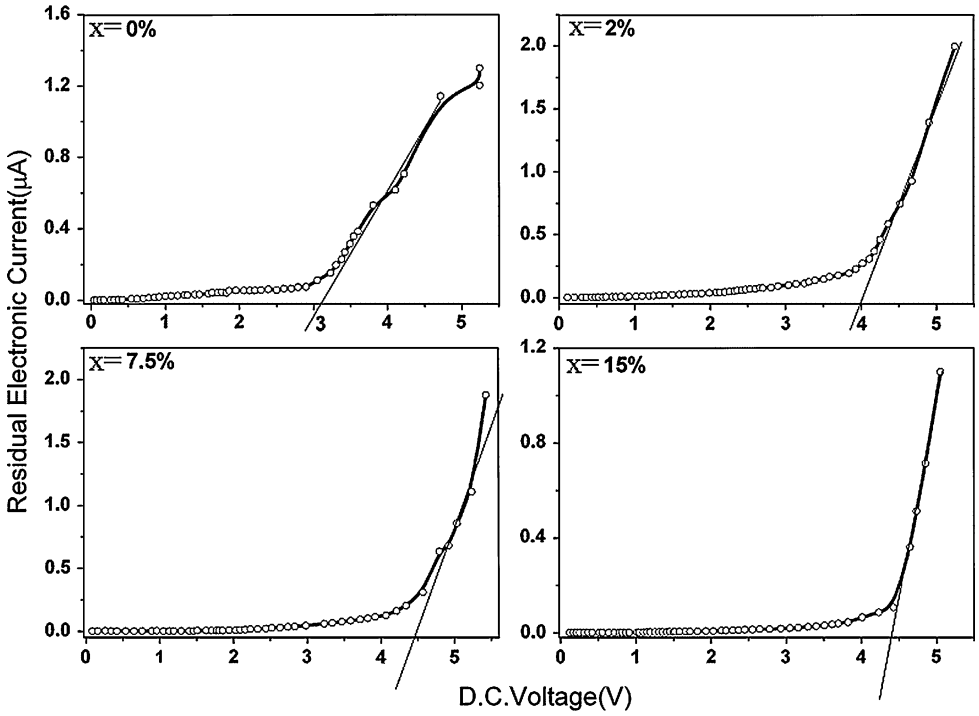

Fig. 11 Variation of residual electronic current as a function of applied d.c. voltage for PNCE films of composition $PMMA_4$–$LiClO_4$ + *x* wt% nano-YSZ

Step 1

The molecular structure of PMMA comprises of two electronegative sites (C=Ö, O–CH_3) with which the cation (Li^+) coordination is possible (Fig. 12ai). Since the carbonyl (C=Ö) group has stronger electron donicity than O–CH_3 within the PMMA structure, Li^+ ion form coordinate bond with the Ö atom of the carbonyl group (C=Ö). This possibility has been confirmed in the FTIR results and reported by us [25]. Hence, the C=Ö is the only site in the structure of PMMA monomer units where the Li^+ coordination seems feasible. It is shown schematically in Fig. 12aii. In case of pristine PMMA–$LiClO_4$ (PS) matrix, a Li^+ cation having coordination number ~ 5 may be expected to form coordinate bond with a maximum of five electron rich carbonyl oxygen (C=Ö) sites in the polymer host matrix. It seems a reasonable possibility in view of the Lewis base character of the PMMA chain that favours polymer–ion interaction [31]. This polymer cation (Li^+) interaction may occur in any of the following ways:

(i) Direct coordination of cation with C=Ö of the polymer chain as depicted in (Fig. 12bi).
(ii) Cation (Li^+) coordination in with the C=Ö group of polymer chain via an anion in between two such chains. This is shown in Fig. 12bii.

Step 2

The nanoscopic filler (n-YSZ) has a high (surface/vol) ratio as well as an inherent Lewis acid group behaviour that facilitates its interaction with the cation coordinated polymer chain behaving like a Lewis base. As a consequence, dispersion of the nanocrystalline YSZ filler into the PS

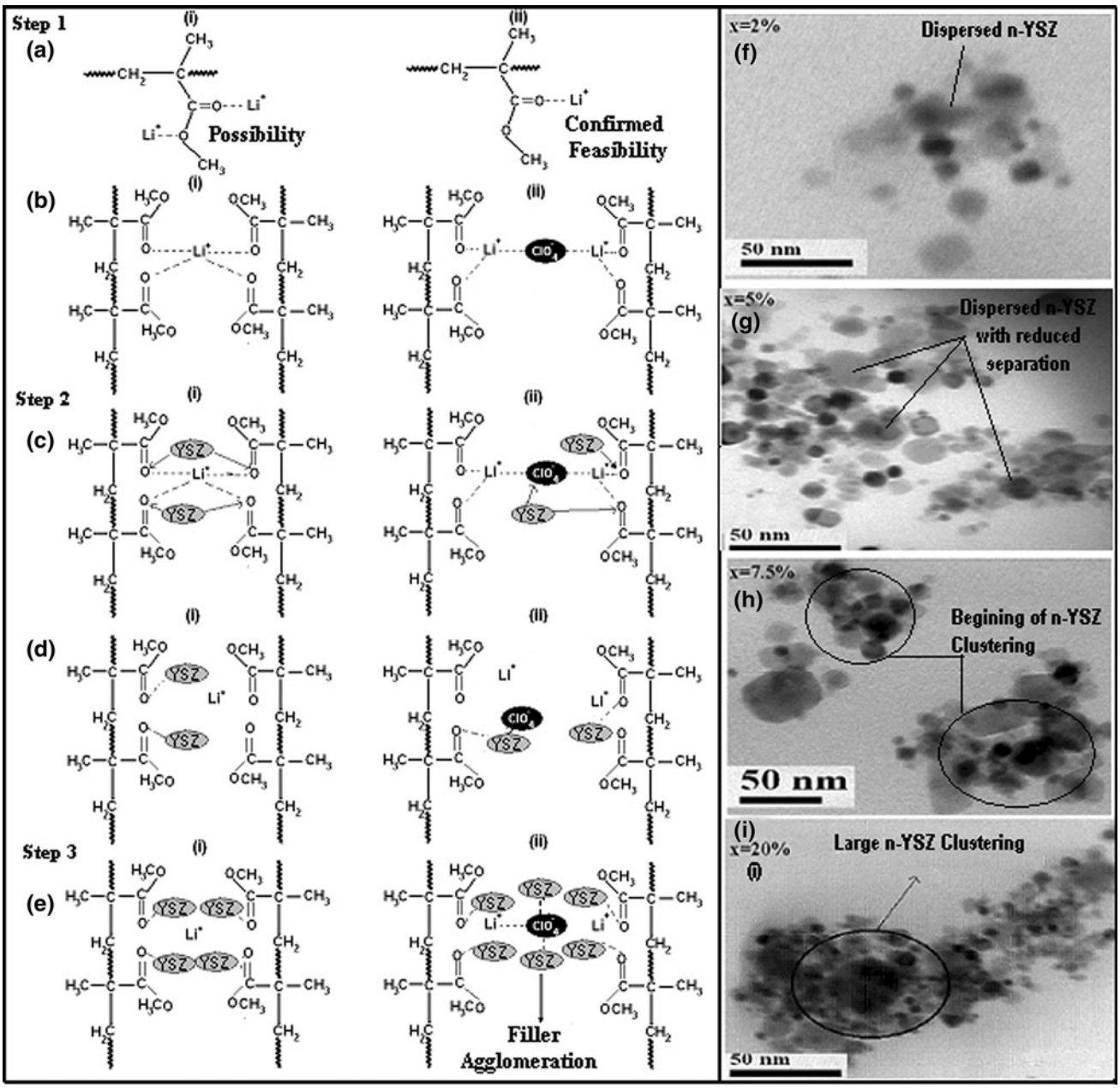

Fig. 12 **a–e** Scheme showing filler–ion interaction and proposed mechanism for ion transport in the PNCE films, TEM micrographs for PNCE films with **f** $x = 2$ wt%, **g** $x = 5$ wt%, **h** 7.5 wt% and **i** 20 wt%

matrix causes n-YSZ interaction with both Li^+ cations attached to C=Ö group of PMMA or with ClO_4^- anions. These possibilities are shown in Fig. 12c (i and ii). The FTIR results in the present studies have indicated feasibility of n-YSZ interaction with the C=Ö group of PMMA. As the addition of even a small amount of n-YSZ the peak at 1728 cm^{-1} and also the shoulder at 1665 cm^{-1} shifting towards lower side and also broadening (Fig. 4a). Hence, the changes in the FTIR results suggest convincing evidence for filler–polymer interaction. Further, the high dielectric permittivity and hard Lewis acid character of the n-YSZ filler affects weak coordinate bond between Li^+ and C=Ö due to filler–polymer interaction. This causes release of Li^+ ion as free mobile charge carrier resulting in enhancement of the available free charge on immediate addition of the filler particles (i.e. low concentration 1–2 wt%). The possible situations are shown in Fig. 12d (i and ii). Such an ion–filler interaction has been evidenced in the FTIR results (Fig. 9). It leads to an increase in the number of mobile charges in the PNCE matrix.

The relative increase in the number of available free mobile charge carriers has also been estimated from the

FTIR profile of $\delta_a(ClO_4^-)$ shown in Fig. 9. This enhancement of free mobile charge carriers causes a significant increase in the electrical conductivity that appears to be consistent and logical in accordance with the relation

$$\sigma = \sigma_{cation} + \sigma_{anion} = \sum_i \mu_i q_i n_i,$$

where n_i is the fraction of free anion/cation as proposed by Kohlgaush for infinitely diluted electrolytes.

Step 3

As the filler concentration increases, the number of free mobile charge carriers decreases due to a number of possibilities such as: (1) immobilization of anion (ClO_4^-) because of its interaction with nano-YSZ, (2) formation of ion pair/higher ion aggregates, and (3) entrapment of free ionic species in the localized clusters at high concentration of n-YSZ (Fig. 12e (i and ii)) The clustering of nanofillers has also been physically visualized in the TEM micrograph for composite matrix with increase in the filler loading. At 5 wt% n-YSZ, the distance of separation between filler particle decreases (Fig. 12g). As the concentration reaches 7.5 wt% cluster of nanofillers begin to be visible (Fig. 12h). The effect of multiple clustering of nanofillers is clearly seen in the TEM micrograph for composite matrix at higher filler loading of 20 wt% (Fig. 12i). The overall effect of nanocluster formation at higher filler loading is immobilization of charge carriers leading to a relative lowering in d.c. conductivity at higher filler loading.

Conclusions

Dimensionally stable ion conducting PNCE series of films based on $PMMA_4$–$LiClO_4$ dispersed with different concentration of nano-YSZ is reported. Dispersed phase nanocomposite formation has been confirmed from the XRD analysis. Effect of nano-YSZ dispersion in ion–ion and ion–polymer interaction has been investigated using FTIR. The result from FTIR agrees well with electrical conductivity variation with n-YSZ concentration. The evidences of ion dissociation have been observed at very low concentration of the nanofiller, which, inturn, causes of more number of free charge carriers. A higher fraction of free mobile charge carrier at low filler loading appears to be well correlated with the variation of electrical conductivity. Electrical conductivity enhancement on n-YSZ dispersion occurs by $\sim$2 orders of magnitude at 30 °C and by $\sim$5 orders of magnitude at 100 °C when compared with room temperature conductivity for the undispersed PS film. The highest achieved conductivity value is $\sim 1.3 \times 10^{-4}$ S cm^{-1} at 100 °C for 2 wt% n-YSZ. The ionic transport number for all the PNCEs has been estimated to be $\geq$99%. An improvement in voltage stability up to 4.5 V has also been noticed with addition of filler. An ion conduction mechanism has been proposed to explain filler concentration dependent conductivity variation in the PNCE films. This approach seems logical in view of the prevailing Lewis acid–base interaction which causes the release of a fairly high amount of charge carriers at a relatively lower concentration of the filler. However, at high filler concentration ($\geq$7.5 wt%), a complex mechanism occurs due to combined effect of filler–ion interaction, ion pair formation and entrapment of the mobile charges carriers due to local clustering of high surface area filler. The concept of the proposed mechanism is supported by experimental evidences from FTIR and TEM analysis.

Acknowledgement One of the authors (NS) acknowledges with thanks the financial support received from the Council of Scientific and Industrial Research (CSIR), Government of India, New Delhi for carrying out the research at the Department of Physics and Meteorology, Indian Institute of Technology (IIT), Kharagpur 721302, India.

References

1. Wieczorek W, Stevens JR, Florjanczyk Z (1996) Solid State Ion 85:67
2. Sun HY, Sohn HJ, Yamamoto O, Imanishi N (1999) J Electrochem Soc 146:1672
3. Kumar B, Scanlon LG (1999) Solid State Ion 124:239
4. Pandey GP, Hashmi SA, Agrawal RC (2008) Solid State Ion 179:543
5. Jiang G, Maeda S, Saeto Y, Tanase S, Sakai T (2005) J Electrochem Soc 152:767
6. Long Y, Shanks RA (1996) J Appl Polym Sci 61:1877
7. Misra RKD, Nerikar P, Bertrand K, Murphy D (2004) Mater Sci Eng A 384:284
8. Bartczak Z, Argon AS, Cohen RE, Weinberg M (1999) Polymer 40:2347
9. Dissanayake MAKL, Jayathilaka PARD, Bokalawala RSP, Albinsson I, Mellander BE (2003) J Power Sources 409:119
10. Capiglia C, Mustarelli P, Quartarone E, Tomasi C, Magistris A (1999) Solid State Ion 118:73
11. Mohapatra SR, Thakur AK, Choudhary RNP (2009) J Power Sources 19:601
12. Weiczorek W, Florjanczyk Z, Stevens JR (1995) Electrochem Acta 40:2251
13. Przyluski J, Siekierski M, Wieczorek W (1995) Electrochim Acta 40:2101
14. Croce F, Appetecchi GB, Persi L, Scrosati B (1998) Nature 394:456
15. Croce F, Persi L, Ronci F, Scrosati B (2000) Solid State Ion 135:47
16. Bhattacharya R, Phaniraj TN, Shailaja D (2003) J Membr Sci 227:23
17. Xuan X, Wang J, Tang J, Qu GL (2000) J Spectrochim Acta A 56:2131
18. Wang Z, Huang B, Huang H, Chen L, Xue R (1996) Solid State Ion 85:143

19. Chabanel M, Touaj KJ (1996) Chem Soc Farad Trans 92:4207
20. Mishra HK, Parida KM (1999) Appl Catal A 184:219
21. Kumar R, Sharma JP, Sekhon SS (2005) Eur Polym J 41:2718
22. Stuart BH (2004) Infrared spectroscopy: fundamentals & applications. Wiley, New York
23. Licoccia S, Trombetta M, Capitani D, Proietti N, Romagnoli P, Vona LD (2005) Polymer 46:4670
24. Kumutha K, Alias Y (2006) Spectrochim Acta A 64:442
25. Shukla N, Thakur AK (2009) Ionics 15:357
26. Romagnoli P, Trombetta M, Silvia L (2004) J Eur Ceram Soc 24:1153
27. Berthier C, Gorecki W, Minier M, Armand MB, Chabagno JM, Rigaud P (1983) Solid State Ion 11:91
28. Chabanel M, Touaj KJ (1996) Chem Soc Faraday Trans 92:4207
29. Hsu CS, Mansfeld F (2001) Corrosion 57:747
30. Wang SJ, Ong CK, Xu SY, Chen P, Tjiu WC, Huan ACH, Yoo WJ, Lim JS, Feng W, Choi WK (2001) Semicond Sci Technol 16:L13
31. Bruce PG (1995) Electrochim Acta 40:2077